LUND
UNIVERSITY

Transient photocurrent measurements on Polymer Solar Cells

A study of how device physics changes when dynamical excitation conditions as repetition rate and pulse energy is varied

Unn Dahlén

2012-02-15

Supervisors: Arkady Yartsev and Dimali Vithanage

Abstract

Organic solar cells made of polymers are an attractive alternative to the conventional solar cells which are commercially used today. The polymer solar cell is cheap to produce, due to the high absorption coefficients which limits the needed thickness of the material and due to the simple manufacturing process, which doesn't demand high temperatures. However, the efficiencies of polymer solar cells are yet too low for commercial production. To optimize the efficiency a critical step is to understand the overall mechanism of the conversion from photon energy into electric and what factors limit the conversion.

In this report studies on the device physics of two different polymer solar cells were performed by time resolved electrical traces in terms of *EQE**. Pulsed laser was used as a light source. The aim with the study was to investigate how dynamical excitation conditions as repetition rate and pulse energy influence on the solar cell device physics. To specify the investigation the following questions were asked: Are there any limits of solar cell performance regarding concentration of photons incident on the solar cell? If yes, what are the limits? And in regarding repetition rate; does the solar cell need to establish some quasi-equilibrium distribution of photo-generated charges in order to optimize the solar cell performance?

A substantial part of this project involved the set up of a program which would enable the analyses of the solar cell response and put the data into a fit.

It is shown that the pulse energy is substantial for the conversion of photons into electrons. For high pulse energies (~10^{11}-10^{13} *hv*) the *EQE** starts to decreases and this is attributed to an increased contribution from non-geminate recombination. Shortly above the pulse energy 10^{14} *hv* the limit for solar cell operation is reached. No lower limit for solar cell operation regarding pulse energy was found in the energy range measured. As for the repetition rate, it's shown that no significant change in the physical processes of the solar cell can be deduced when the frequency is varied in a range of 1000 Hz to 25000 Hz. This is interpreted as there is probably no need to establish a quasi-equilibrium of photo generated charges to optimize the solar cell efficiency.

**EQE is the external quantum efficiency which is the ratio between incoming photons and extracted electrons from the solar cell. See also 2.1.2 External quantum efficiency in the theory section.*

Sammanfattning

Organiska solceller gjorda av plast är ett attraktivt alternativ till de konventionella solceller som används idag. Plastsolcellerna är billiga att producera, dels på grund av deras höga absorptionsförmåga, vilket medför att solcellerna kan göras tunna och dels på grund av den enkla produktionsprocessen, som inte kräver några höga temperaturer. Än så länge är plastsolcellernas verkningsgrad för låg för kommersiell produktion. För att optimera verkningsgraden krävs kunskap om hela omvandlingsprocessen från fotonenergi till elektrisk energi och vilka faktorer som begränsar processen.

I den här rapporten görs studier av den fysikaliska processen i två olika organiska solceller genom att undersöka den tidsupplösta elektriska responsen i termer av den externa kvanteffektiviteten. Pulsade laser användes som ljuskälla. Syftet med studien var att undersöka hur excitationsvillkor som frekvens och pulsenergi påverkar de fysikaliska processerna i solcellen. Ett antal frågor ställdes för att specificera undersökningen: Finns det någon begränsning för solcellens prestationsförmåga vad gäller den initiala koncentrationen av fotoner på solcellen? Om ja, vilka begränsningar? Och angående frekvensen; behöver solcellen bilda en kvasijämviktsfördelning av fotogenererade laddningar för att optimera solcellens prestanda?

En stor del av detta projekt involverar utvecklingen av ett program som kunde möjliggöra analysen av solcellens respons samt på ett bra sätt presentera resultaten.

Det visar sig att pulsenergin har betydelse för omvandlingsprocessen i solcellen. Vid höga pulsenergier (~10^{12}-10^{13} *hv*) sjunker den externa kvanteffektiviteten och detta tillskrivs den icke parvisa återföreningsprocessen. Strax ovanför pulsenergier av storleksordningen 10^{14} *hv* nås begränsningen av solcellens funktion. Ingen nedre begränsning nås i det intervallet av pulsenergier som undersöks i denna rapport. När det gäller frekvensen, visar det sig att ingen signifikant förändring av de fysikaliska processerna i solcellen kan utläsas när frekvensen varieras över intervallet 1000 Hz-25000 Hz. Detta tolkas som att ingen kvasijämvikt av fotogenererade laddningsbärare behöver etableras för att optimera solcellens effektivitet.

1 Introduction

1.1 Background

The consumption of energy has been accelerating over the last decades alongside the development of new technologies accompanied with new lifestyles. The effects on the environment due to human activities have been under dispute and the discussion of global warming as a consequence of a larger amount of carbon dioxide in the atmosphere is an up-to-date issue. As a consequence, the search for new renewable energy sources has become high priority and the sun is the only direct energy source to consider.

Solar cells are photovoltaic devices which convert electromagnetic radiation from the sun to electricity. The commercial solar cell today is made of inorganic material, mainly by silicon and is expensive to produce. Organic solar cells, based on conjugated polymers, can be easily processed at room temperature using inexpensive technologies, which makes them an attractive alternative to the expensive inorganic solar cells. Moreover, as the absorption coefficient is high, the films can be made into thin panels and have the added advantage of being flexible. Although there has been fast development of the organic solar cell field with device efficiency improving from less 1% to 9.3 % [1] within the last few years, the efficiency is still very low compared to inorganic photovoltaics. However, the interest of organic solar cells remains high since the cost of organic is much lower than of inorganic solar cells.

The polymer solar cell device function is based on donor and acceptor materials in contrast with inorganic solar cells which relay on p-n junctions. The photo active layer of the solar cell absorbs light and creates excitons which are bound electron-hole pairs. These are separated into free charge carriers and are then transferred to electrodes to extract the current. To optimize the efficiency of the organic solar cell a critical step is to understand the overall mechanism of the conversion of photons to electrons and the recombination processes and other factors that limit the photocurrent out from the device.

1.2 Aim

In relation to solar cell functioning, there are a few questions regarding the conditions of cell illumination.
Are there any limitations for solar cell operation related to the incident light level?
What happens when there is too much light? And what light level is too much? Is it necessary to establish a quasi-equilibrium distribution of photo-generated charges in a cell before efficiency of light-to-electricity conversion will reach its optimal value? Can it be too little light?
Going to the limit of this question, would a solar cell work as efficient for a single incident photon as for a normal sun light illumination?

The main purpose of this project is to answer these questions by investigating the device physics of

two different kinds of polymer-fullerene BHJ solar cell, APFO3:PCBM and TQ1:PCBM60, when illumination conditions are varied. Device measurements would for this project mean extensive analysis of time-resolved electrical traces in terms of *EQE* under varying parameters of the pulse energy and repetition rate. Additionally a program was needed to make the data presentable and put them into a fit. This would enable the user quickly to know the state of the measurements.

1.3 Abbreviations

Abbreviations which are commonly used in literature and through out the text is listed in table 1.1 below.

Table 1.1: List of common abbreviations used throughout the text.

FF	fill factor
HOMO	highest occupied molecular orbital
LUMO	lowest unoccupied molecular orbital
EQE	external quantum efficiency
IQE	internal quantum efficiency
ITO	indium tin oxide
PEDOT:PSS	poly(ethylene-dioxythiophene) doped with polystyrene-sulfonic acid
LiF	lithium fluoride
BHJ	bulk hetero-junction
PCBM	1-(3-methoxycarbonyl) propyl-1-phenyl[6,6]C_{61}
PPV	poly (*para*-phenylene vinylene)
MEH_PPV	poly[2-methoxy-5-(2-ethyl-hexyloxy)-1,4-phenylene-vinylene]
APFO3	poly[2,7-(9,9-dioctylfluorene)-alt-5,5-(4',7´-di-2-thienyl-2´,1´,3- benzothiadiazole)]
TQ1	poly[2,3-bis-(3-octyloxyphenyl)quinoxaline-5,8-diyl-alt-thiophene-2,5-diyl]

2 Theory

2.1 Solar cell parameters

A solar cell is a device which creates electricity upon exposure of light by the photovoltaic effect. Even though the operation principle is different for different types of solar cell the *I-V* (current-voltage) characteristic, shown in figure 2.1, has a similar shape. I_{sc} is the short circuit photo current which flows when opposite electrodes of a solar cell are shortened. V_{oc} is the open circuit voltage, i.e. the voltage when the solar cell electrodes are not connected to an electrical circuit.

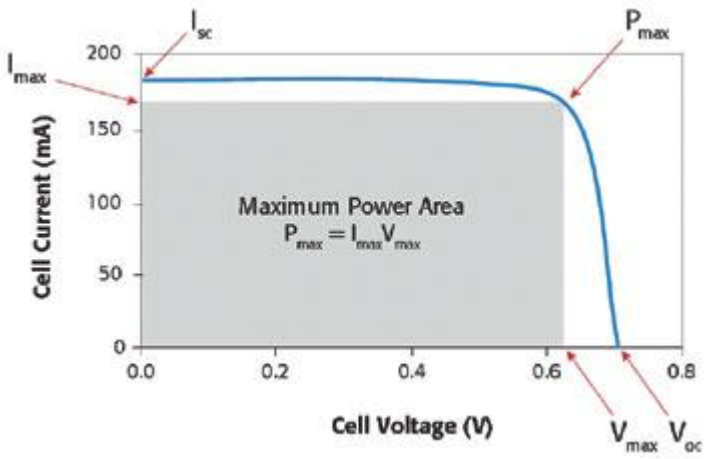

Figure 2.1: Typical IV-characteristics for a forward biased solar cell.

2.1.1 Power conversion efficiency

The power conversion efficiency of a solar cell, η, is the ratio between the maximum power generated by the device, P_{max}, and incident power, P_{in}, due to light input.

$$\eta = \frac{P_{max}}{P_{in}}$$

The power generated from the device is given by the voltage times the current. The maximum power P_{out} is therefore calculated from the point on the *I-V*-curve which gives the largest area within the curve

$$P_{max} = I_{max} \cdot V_{max}$$

This can also be expressed as

$$P_{max} = I_{sc} \cdot V_{oc} \cdot FF$$

where *FF* stands for fill factor and is a ratio between the maximum obtainable power from a device and the power generated with short circuit current I_{sc} and open circuit voltage V_{oc}.

2.1.2 External Quantum Efficiency (*EQE*)

The External Quantum Efficiency (*EQE*) is the ratio of the number of charges extracted from the solar cell to the number of photons shining on the solar cell.

$$EQE = \frac{\#\ extracted\ electrons}{\#incident\ photons}$$

The *EQE* is therefore dependent on both light absorption and charge extraction.

2.1.2 Internal Quantum Efficiency (*IQE*)

The Internal Quantum Efficiency (*IQE*) is the ratio of the number of charges extracted from the solar cell and the number of photons absorbed in the solar cell.

$$IQE = \frac{\#\ extracted\ electrons}{\#absorbed\ photons}$$

The *IQE* is only related charge extraction.

2.2 Polymer solar cell

A polymer solar cell uses a conjugated polymer as a photoactive material. A conjugated polymer is a disordered material with chains of monomers characterized for having an alternating single bond-double bond structure and carbon atoms that are generally sp^2- hybridized.

Single- and double bond

When a pair of electrons is shared by two atoms the resultant bonding is referred as a covalent bond. Sigma (σ) bond and pi (π) bonds are two types of covalent bonds. Sigma bond, also called single bond, is the strongest type of covalent bond formed by head-on overlapping between atomic orbitals. Pi bond is a weaker covalent bond, formed when two lobes of an atomic orbital overlap with two lobes of another atomic orbital. This may occur for pi orbitals which then overlap in parallel. A double bond consists of both a sigma bond and pi bond and is stronger than a single bond.

Sp2-hybridized

Hybridization is a concept which is used in order to explain the bonding properties of molecules made from carbon, nitrogen and oxygen. Hybridized orbitals are assumed to be mixtures of atomic orbitals superimposed on each other. A sp^2-hybridized system has a single p_z-orbital and three hybridized sp^2 orbitals. The sp^2 orbitals form sigma bonds with adjacent atoms in a plane ortoghonal to the p_z-orbital.

In conjugated polymers the electrons from the p_z-orbitals of each carbon atom form collectively the p_z band. The electrons in this band are delocalized and thus the material has a large electronic polarizability. The half filled p_z band are further split into the bonding π and anti bonding π^* bands, due to Peierls instability [2], see figure 2.2. In the following text the π and π^* bands will be called the HOMO respectively the LUMO within the polymer. The characteristics of a conjugated polymer enable

both absorption in the visible region, due to a band gap of approximately 2 eV and electronic charge transport, due to the material polarizability.

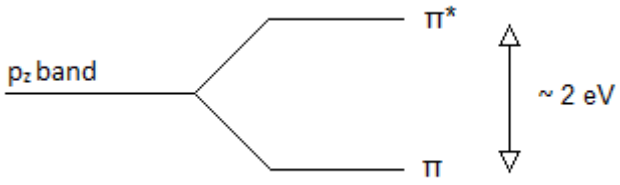

Figure 2.2: Energy levels in a conjugated polymer. Upon light absorption electrons may be excited from the bonding π into the antibonding π band.*

The main advantage of polymer solar cells is that they can be processed from solution at room temperatures onto substrates using simple coating methods. This is achievable by introducing soluble side-chains to conjugated polymers which make them readily dissolved in organic solvents. It's also possible to modify the band gap with changes in the synthesis, making it feasible to regulate the electronic properties.

2.2.1 Working principle

Converting solar light into useful electric power primary requires generation of positive and negative charge carriers and some driving force which can make the current flow through an external circuit.

In organic solar cells incident light absorbed within the photo active layer leads to the creation of an exciton, which is a Coulombically bound electron-hole pair. Primarily the absorption corresponds to the excitation from the highest occupied molecular orbital (HOMO) to the lowest unoccupied molecular orbital (LUMO) within the polymer. In order to generate free charge carriers, the exciton most be separated in to its elementary parts. The exciton diffuses generally 5-20 nm during its lifetime, and in order to separate the exciton into its components it has to reach a dissociation site within its lifetime. Whether it reaches the dissociation site or not depends on the *mobility* of the material, the *lifetime* and the *distance* to the dissociation site. In current organic solar cells the dissociation happens in the interface between an electron donor- and electron acceptor-material. The difference in ionization potential and electron affinity between these materials form a gradient of the potential which induces charge transfer between these materials. The electron is transferred to the acceptor material and the hole remains in the donor material, see figure 2.3.
The final step is the transfer of the charge carriers to respective electrodes. For holes the transport occurs within the donor material and for electrons within the acceptor material. The more separate paths the donor and acceptor have, the less probability of recombination. The prior driving force for the transfer within the active area is the difference in work function of the electrodes. The build in field causes the free charges to hop from site-to-site until they reach their respective electrode. Diffusion due to concentration gradients of hole and electrons affects the drift of charge carriers [2, 3].

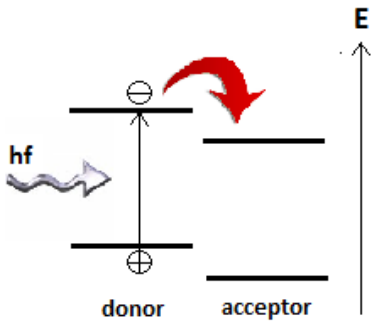

Figure 2.3: Illustration of charge transfer upon light absorption. After excitation from HOMO to LUMO within the polymer (donor) the electron is transferred to the LUMO of the acceptor due to the lower potential. A hole is left in the HOMO of the donor.

2.2.2 Device architecture

The device architecture of a polymer solar cell is shown in figure 2.4. The active material is usually sandwiched between two electrodes with additional layer in between for better charge extraction. The light is incident on the substrate electrode which is both transparent and conducting. Typically substrate is glass covered with a transparent conducting oxide, in general indium tin oxide (ITO). Next layer is PEDOT:PSS , poly(ethylene-dioxythiophene) doped with polystyrene-sulfonic acid. This layer sets the work function of the bottom electrode and improves the surface quality and the hole injection/extraction. On the other side of the active layer (the back of the solar cell) there is a metal electrode, in general aluminum, with the ability to reflect transmitted light back through the active material. This electrode has a lower work function compared to the substrate electrode. Improvements in open circuit voltage and fill factor has additionally been observed with a thin layer (thickness 0.6 nm) of lithium fluoride (LiF) at the aluminium electrode, although the reason is not fully understood [2, 4, 5].

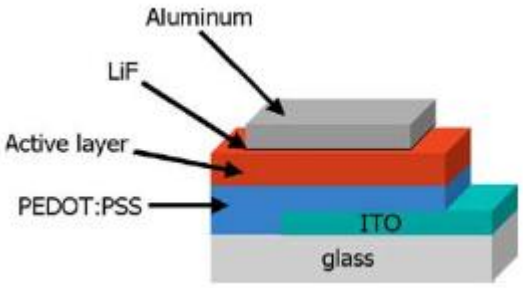

Figure 2.4: General device structure of a polymer solar cell.

2.2.3 Active layer

The structure of the *active layer* has strong impact on the solar cell performance and usually three different types of devices are mentioned: Single layer device, bilayer device and bulk hetero-junction device.

Single layer device

In a single layer device the active material is a conjugated polymer and the dissociation of electron-

hole pair is limited to the vicinity of the metal electrode. Since the diffusion length in the polymer limits the number of exciton which reaches the dissociation zone only a small fraction of the total generated excitons will contribute to the photocurrent.

Bilayer device

In a bilayer device the active material consists of two layers, one with the donor (polymer) and one with the acceptor. The exciton dissociation takes form in the interface between the two layers and since the hole stays in the donor and electron in the acceptor the charge carriers can travel within separate materials, which reduces the likelihood of recombination. Also here the exciton diffusion length limits the number of excitons reaching the dissociation zone and therefore the extracted photocurrent.

Bulk hetero-junction device (BHJ)

The most abundant type of polymer solar cell today is the Bulk hetero-junction solar cell. In this device the active material is a blend of acceptor- and donor-species, forming an interpenetrating network on the nanometer scale. To form the layer the acceptor and donor are resolved in a common solvent which then is deposited using different coating techniques. The phase separation between the two components occurs when the solvent rapidly evaporates and typical separation distances are 10-20 nm [4]. In this complex network, the exciton diffusion length is of the same order of magnitude as the phase separation between donor and acceptor. The exciton diffusion length is defined as the length the exciton propagates in the active material within its mean lifetime. Only a fraction 1/*e* of the initial number of excitons will therefore have travelled the diffusion distance. Since the probability of charge separation is close to unity [5] it follows that there are not pure faces through the active material, but a mixed interpenetrating network of acceptor and donor material. It is also worth saying that the generation of photocurrent is no longer limited to a specific part of the active area, but the dissociation can take part through the whole volume of the active material. However, interpenetrating network leads to a lower mobility due to the increased disorder and the traverse pathways of holes and electrons result in increased recombination. Despite all negative effects the introduction of BHJ in the early 90's has lead to higher power efficiencies [2].

2.2.4 Internal electric field and open circuit voltage

The work function of a metal is defined as the difference in potential energy of an electron between the vacuum level and the Fermi level. The vacuum level is the energy of an electron at rest at a point infinitely far away from the metal. The Fermi level is defined as the energy of the topmost filled orbital at absolute zero in the material.

The device function of a thin organic solar cell can in general be simplified using the metal-insulator-metal (MIM) model. This is valid as long as the organic semiconductor is not doped and as long as no space charge exist [2]. Before the device is assembled the metal and oxide layer (*ITO*) have different work functions and therefore different Fermi levels, see figure 2.5 (A). When the polymer solar cell is put together charge carrier start to diffuse to align the Fermi levels of the layers and establish a thermal equilibrium. Since the polymer is an insulator (according to the MIM-model) only charge carriers from the electrodes are able to diffuse. Electrons will flow from the low to the high work function ITO electrode and this will leave the low work function electrode positive and the high work

function electrode negative. The potential difference between the electrodes will result in a linear electric field, see figure 2.5 (B). It is this field that assists in the dissociation of the bound charge carriers and transfers the hole to the ITO electrode and the electron to the Aluminum electrode.

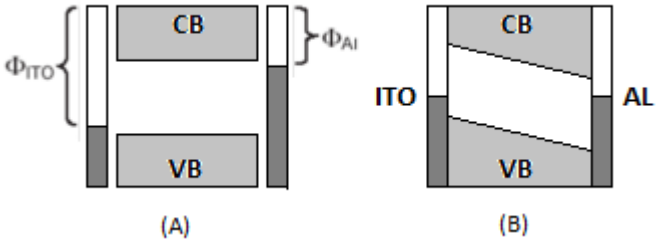

Figure 2.5: (A) Before the device is assembled the work function of Aluminum is lower than the work function of ITO. (B) Work functions aligned and a linear electric field is established. VB and CB is the valence band and conducting band respectively of the polymer.

The *open circuit voltage* in polymer solar cells is primarily limited by the difference of the charge carrier energy levels:

$$V_{OC1} < LUMO_{acceptor} - HOMO_{donor}$$

Secondly by the difference in work function between the electrodes:

$$V_{OC2} < work\ function(PEDOT{:}PSS) - work\ function(Al)$$

A linear relationship between measured open circuit voltage and HOMO position in the donor respectively LUMO position in the acceptor has been observed. The open circuit voltage has been shown also to have a linear dependence on the difference in work function of the electrodes. According to the paper by Blom et al "Device physics of Polymer-Fullerene BHJ Solar Cells" [3] the latter linear dependence holds only when the Fermi levels of the contacts are within the band gap of the semiconductor and when the contacts are not in close align with the charge carrier energy levels. If they are, the contacts are ohmic and there will be charge transfer of electrons or holes from the electrodes into the semiconductor in order to align the Fermi levels. This will result in pinned work functions close to the LUMO of the acceptor and HOMO of the donor, and the V_{oc} will be approximately governed by the difference between these two levels [2].

2.3 Polymer-Fullerene solar cells

In a polymer-fullerene solar cell the donor is a conjugated polymer while the acceptor is a fullerene. In 1992 Sariciftci et al. introduced buckminsterfullerene (C_{60}) which has had a great impact on the development of polymer solar cells. Upon light excitation efficient charge transfer from a conjugated polymer (MEH_PPV) to the fullerene could be seen and since then a number of investigations concerning buckminsterfullerene have been done. Wudl et al. synthesized a soluble derivative of C_{60}, PCBM (1-(3-methoxycarbonyl) propyl-1-phenyl[6,6]C_{61}) and this fullerene is commonly used in polymer-fullerene solar cells today [2, 4]. Another important pusher for the BHJ devices was Heeger, who got a high efficiency out from the bicontinuous network of donor- acceptor heterojunctions [7].

2.3.1 Physical processes in a Polymer-Fullerene BHJ device

The fundamental physical processes in a BHJ device can be divided into following five steps (illustrated in figure 2.6):

(1) Photon absorption
(2) Exciton diffusion
(3) Exciton dissociation
(4) Charge transfer
(5) Charge extraction at electrodes

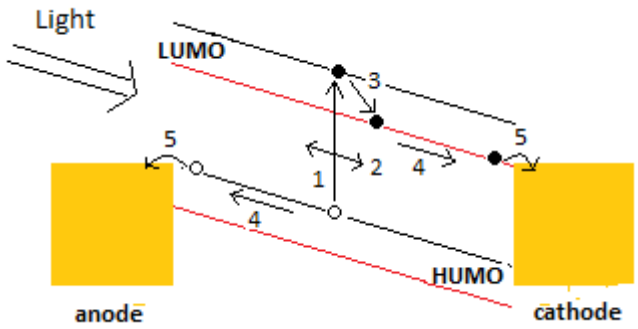

Figure 2.6: Illustration of fundamental physical processes in a bulk hetero-junction device. The HUMU and HOMO are represented with red lines for the acceptor and black lines for the donor.

Photon absorption
Light is primarily absorbed in the conjugated polymer of the active material which leads to the creation of excitons. The main limit for the photon absorption is the band gap in the polymer. Only incident light with energy larger than the band gap is absorbed within the active material. Since conjugated polymers have a band gap generally around 2 eV this limits the possible sun photon absorption to about 20%. The photon absorption also varies with absorption coefficient and thickness of the active area. The absorption coefficient is relatively high in organic semiconductors (ca. $10^5\,cm^{-1}$) and consequently the active area can be relatively thin, a few hundred nanometers or smaller. Another loss is the reflection of photons at the surface of the solar cell, which stops the photons before reaching the active material [3].

Exciton diffusion
The exciton diffusion length varies between conjugated polymers in a range from 5 to 20 nm. In order to generate free charge carriers the exciton has to diffuse to a dissociation site within its lifetime. The influencing parameters here are the charge carrier mobility of the polymer, the distance to a dissociation site and the lifetime of the excited state. Since the probability of charge separation is close to unity in BHJ devices [5], this step shouldn't limit the generation of photocurrent.

Exciton dissociation
The binding energy of the exciton is not well defined due to the disorder present in conjugated polymers, but a typical value is 0,4 eV and room temperature is not sufficient enough to dissociate the exciton [3]. The charge transfer happens in the interface between the donor and acceptor

material, due to the difference in ionization potential and electron affinity between the materials. After charge transfer a bound charge pair is formed with a hole in the donor and bound to an electron in the acceptor, this is sometimes called the charge transfer state. From the charge transfer state the bound charge pair can either decay to the ground state or separate into free charge carriers. The probability of charge separation is dependent on both temperature and field, and also the distance between the bound electron and hole which determines the Coulomb force between hole and electron. In order to dissociate the charge carrier hopping distance must be larger than the Coulomb radius [8]. Under short circuit condition (see figure 1.1, 2.1 solar cell parameters) it has been shown that in solar cells based on PPV/PCBM blends only 60 % of the excitons can dissociate and therefore this is a main loss mechanism in the operation of a polymer solar cell. A long lifetime of the charge state would enable more bound electron-hole pair to dissociate [3].

Charge transport

The transport of the charge carriers to the electrodes is limited by recombination. Interaction with atoms and other charges may slow down the travel speed of the charge carriers and result in further recombination [9]. An efficient charge carrier transport to the electrodes requires an interpenetrating network with bicontinuous percolated pathways formed from donor and acceptor phases [8].

Charge extraction at electrodes

The alignment of the electrode work functions with the charge carrier energy levels may influence the charge extraction. When the semiconductor and electrodes are brought together band bending occurs near the contacts. If the work functions of both electrodes are outside both Fermi-levels then blocking contacts are formed and for the charge carriers to be extracted they have to overcome a potential barrier. By changing the potential of the electrode the contact can become non-blocking [9].

2.3.2 Recombination

Consider a polymer solar cell is exposed to light within the absorption spectrum and an exciton is formed by photon absorption. Due to the disorder in the material the hole and electron remain bound. After charge separation the charge carriers are distributed in the active material, but when they arrive within the Coulomb radius of an opposite charge carrier the electron may occupy the hole and thereby eliminate both mobile charge carriers. This is called recombination and there are different types. When an electron occupies the same hole as it was generated together with the recombination is called geminate. When an electron occupies a hole generated together with another electron the recombination is called nongeminate. The latter one is intensity dependent and is commonly simulated with the Langevin model. Geminate recombination is intensity independent and the Onsager model with some refinements is used for simulation of this process [10]. A typical continuity equation is

$$\frac{dn}{dt} = G_0 - \frac{n}{\tau} - \gamma np \qquad (1)$$

where G_0 is the photogeneration term, $\frac{n}{\tau}$ is a monomolecular recombination term and γnp is a bimolecular recombination term. n and p are the electron- and hole density respectively and τ is the

lifetime of the charge transfer state. The recombination strength is $\gamma = \frac{q}{\langle\varepsilon\rangle}\langle\mu\rangle$, where $\langle\varepsilon\rangle$ is the spatially average dielectric constant and $\langle\mu\rangle$ is the averaged sum of the electron and hole mobility [11]. If no space charge exist and the charge carriers are equally distributed throughout the active area then the hole concentration is equal to the electron concentration. The equation (1) then becomes

$$\frac{dn}{dt} = G_0 - \frac{n}{\tau} - \gamma n^2 \qquad (2)$$

Notice that geminate recombination is a first order process while nongeminate recombination is a second order process.

It has been suggested that both geminate and nongeminate recombination and also trapped charges contribute to the recombination in the device of a BHJ solar cell, but there is no general conclusion about the dominating recombination type [12].

2.3.3 Space charge

The hole mobility is in general less than the electron mobility in a BHJ device. If the difference in mobility between the two types of charge carrier is too large, space charge will limit the photocurrent. It has been demonstrated that a critical ratio is when the difference in mobility between the charge carriers exceeds two orders of magnitude [6]. For smaller differences the space charge shouldn't affect the photocurrent significantly. At short circuit condition the electric field is quite strong and charge carriers are readily extracted keeping the density of electrons and holes low throughout the device [10].

2.3.4 Timescales

A schedule illustrating the processes in the active material is shown in figure 2.7. The fastest process in the polymer solar cell is generation of charges (1) which occurs on a timescale in the range 50-100 fs. Since the timescale for the competing process, photoluminescence (2), is much larger photoluminescence quenching will be observed of the otherwise highly luminescent conjugated polymer. Back transfer (3), or recombination of bound charge pairs, occurs on a timescale of µs. This implies that the charge transfer state is efficiently formed and metastable [2]. Recombination of free charges, including both geminate (4) and nongeminate (5) recombination has been observed to occur on timescales of ns or longer [12].

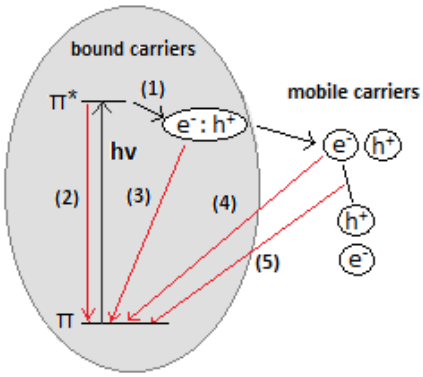

Figure 2.7: Photogeneration of free charges and recombination processes. (1) Charge transfer. (2) photo luminescence. (3) Back transfer: Recombination of bound charge pair. (4) Geminate recombination: Recombination of mobile charge pair. (5) Nongeminate recombination: Recombination of mobile charge carriers.

2.4 Solar cell discharge

The dicharge of a polymer solar cell after exposure of light can be compared with the discharge of a capacitor through a RC-circuit.

An RC circuit with a loaded capacitor and a resistor connected in series is shown in figure 2.8.

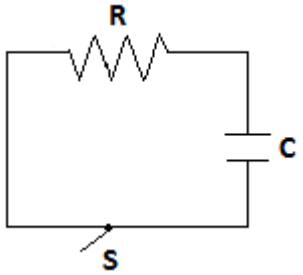

Figure 2.8: An RC-circuit with a resistor (R), capacitor (C) and a switch (S) connected in series. When the circuit is closed the capasitor will discharge through the resistor.

When the circuit is closed the capacitor will discharge through the resistor and according to Kirchoffs law:

$$IR + \frac{Q}{V} = 0 \Leftrightarrow \left(\frac{dQ}{dt}\right)R + \frac{Q}{V} = 0$$

This differential equation can be solved for *Q* as a function of time. The solution is:

$$Q(t) = Q_0 e^{-t/RC}$$

where Q_o is the initial charge on the capacitor. The current as a function of time is found when differentiating this expression:

$$I(t) = -(\frac{Q_0}{RC})e^{-t/RC}$$

where $I_o = Q_o/RC$. As can be seen the capacitor will discharge exponentially and the constant *RC* determines how quickly the capacitor discharges.

In a simplified picture we can imagine the solar cell being the capacitor charged by the laser pulse. The series resistance represents the sum of the resistance from the active area, electrode interfaces and contacts. The current will diminish in the solar cell after excitation due to extraction of charges at the electrodes, but also due to recombination. Geminate recombination is a first order process and consequently the decrease of charge carriers due to geminate recombination will be exponential in time. In the case of nongeminate recombination which is a second order process the decrease will not be exponential. Consequently, when there is no nongeminate recombination or only a weak contribution from this process the current across the solar cell should therefore decline exponentially due to charge extraction and recombination.

3 Method

The method has been divided into two parts to simplify for the reader. In part one the method for the experimental section and theoretical considerations is present and in part two the method for the construction of the analyze program is present. Below follows a short description of the methods.

3.1 Description of method

Part 1

The investigation of the dynamical processes in the polymer solar cells was performed under short circuit condition by transient photocurrent measurements. A pulsed laser with a wavelength of 532 nm was used as a light source. When the light hit the solar cell the devices voltage response was collected with an oscilloscope. In order to relate the experimental fluency to the solar fluency in true operating conditions of a solar cell, an investigation was made to find the laser fluency of photons which corresponds 1 sun in steady state solar light operation (see section 3.1.1 Fluency). Both fluency and repetition rate was varied over the largest range possible in the measurements with the given capacity of the instruments.

Part 2

To calculate and analyze the results a program was made in MATLAB. This program enabled the user to calculate the *EQE* for varied excitation condition. The program also fitted the current discharge of the solar cell with an exponential function in order to relate non geminate recombination to specific pulse energies. Additionally, supplement to the program was made to analyze the deviation of the exponential fit from the raw data.

Part 1

3.2 Theoretical Considerations

3.2.1 Fluency

The sun has a radiation spectra close to a black body of temperature 5800 K. According to Plancks law the irradiance $I(\lambda, T)$ emitted from a black body as a function of temperature, *T*, and wavelength, λ, is given by

$$I(\lambda, T) = \frac{2hc^2}{\lambda^5} \frac{1}{e^{\frac{hc}{\lambda kT}} - 1}$$

where *c* is the velocity of light, *h* is the Planck constant and *k* is the Boltzmann constant. For the sun this implies a high irradiance in the visible part of the electromagnetic radiation spectrum.

The American Society for Testing and Materials (ASTM) has developed a terrestrial reference spectrum for photovoltaic performance [13], shown in figure 3.1. The standard is set by an airmass of 1.5, a tilt of 37° towards the equator and, additionally, atmospheric conditions. Both diffuse and direct components of the radiation are taken into account and the resulting terrestrial intensity is approximately 1000 W/m^2.

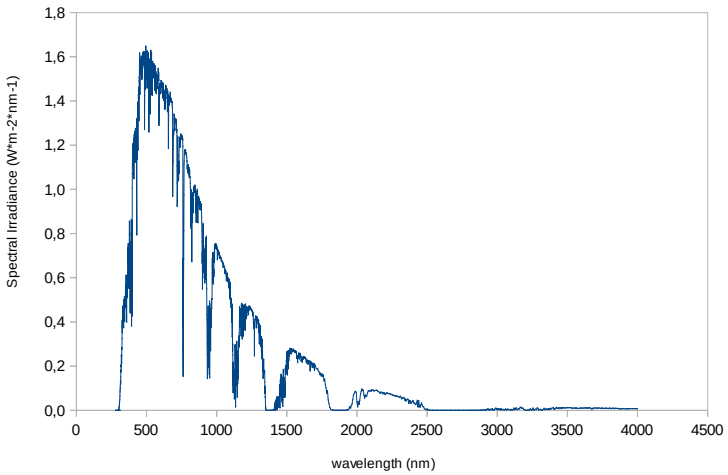

Figure 3.1: AM 1.5 spectrum, tilt 37°.

A polymer solar cell has a band gap of approximately 2 eV which corresponds to the energy of a photon with wavelength 600 nm. It follows that only photons with shorter wavelength than 600 nm will participate in the excitation process within the solar cell.
Figure 3.2 shows a distributionfunction of the AM1.5 solar photon flux (#photons/(s·cm^2)) as a function of wavelength.

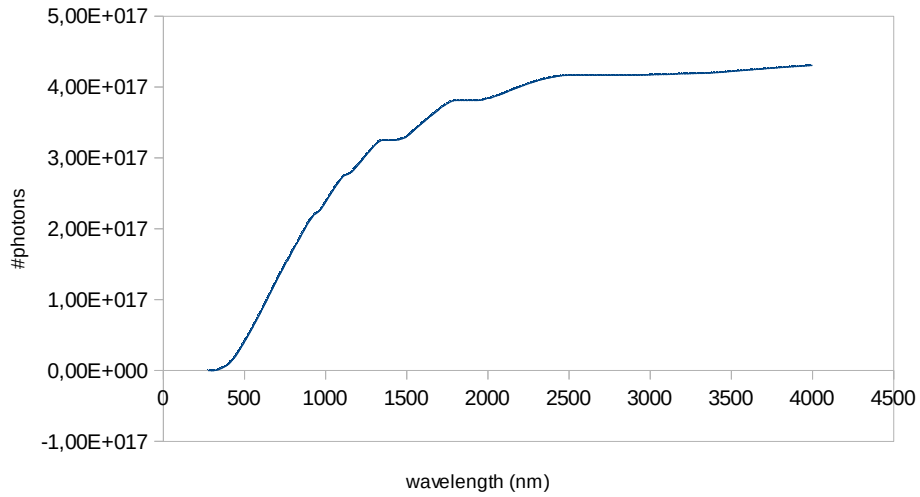

Figure 3.2: AM 1.5 solar photon fluency.

Including all the wavelengths the total photon flux is $4{,}30*10^{17}$ photons/(s · cm^2) and only 20 % of the photons, a number of $8{,}25*10^{16}$, have wavelengths less than 600 nm. Given that a polymer solar cell generally absorbs till ~ 600 nm, it means that only one fifth of the photons are able to contribute to the generation of the photocurrent.

Definition 1 sun
Based on the observations above *1 sun* was defines as the fluency of $8{,}25 \cdot 10^{16}$ *photons/s/cm*^{2}.

In order to compare experimental conditions to the functioning solar cell conditions the investigated interval of the fluency included the fluency defined for 1 sun. The range of the interval was taken as wide as possible to incorporate both geminate and nongeminate recombination.

3.2.2 Active material

The molecular structure of the polymers APFO3, TQ1 and the fullerene PCBM, respectively is shown in figure 3.3. The absorption spectrum for the polymers is shown in figure 3.4.

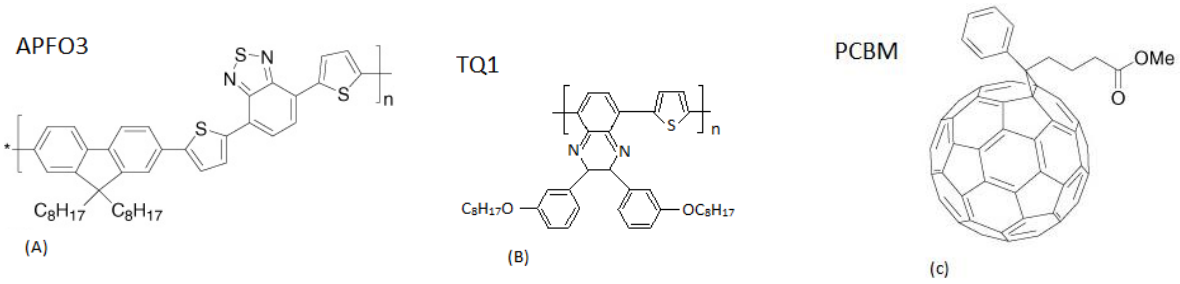

Figure 3.3: Molecule structure for (A) APFO3, (B) TQ1 and (C) PCBM.

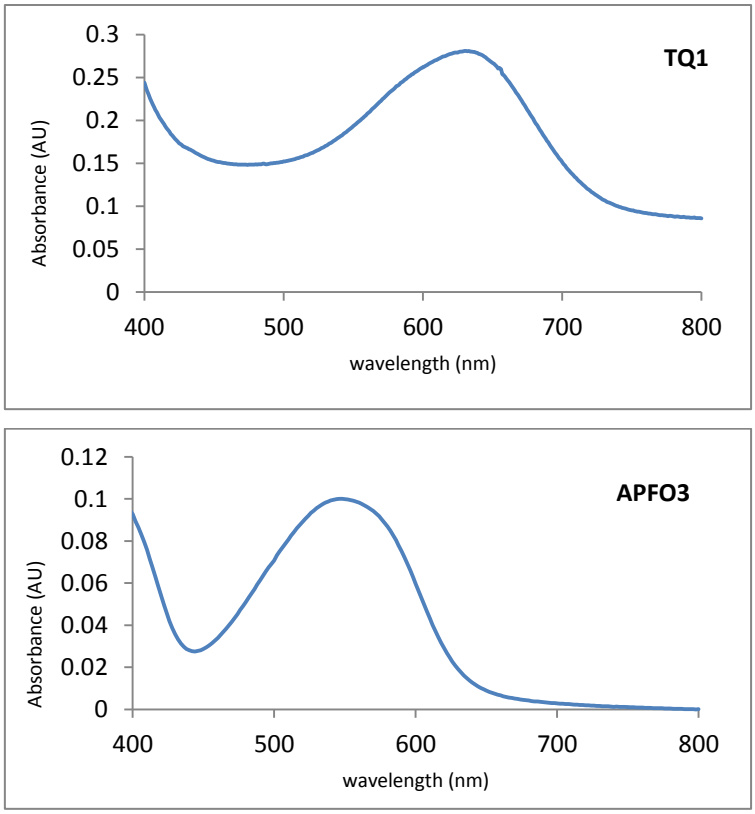

Figure 3.4: Absorption spectrum for topmost: TQ1. Bottommost: APFO3.

The laser used in the experiment had a wavelength equal to 532 nm. This is within the range of both absorption spectrum for the polymers. Since the absorbtion within the active material primarly is due to the polymers the absorption spectrum for the PCBM is not shown. The absorbance spectrum of the polymer doesn't have to be correlated to the resulting absorbtion in the material. Depending on the thickness of the layers in the device reflective waves will interfere either constructicely or destructively. The efficient solar cells have been optimized such that the thickness of layers will contribute to constructive interference within the active material.

3.3 Experimental method

3.3.1 Sample preparation

APFO3:PCBM, ratio 1:4
APFO3 and PCBM were solved in a chloroform solution. The solution was then deposited on a clean glas substrate by spincoating at 1000 rpm in 1 minute.

TQ1-PCBM60, ratio 1:2
TQ1 and PCBM60 were solved in 1,2-Dichlorbenzene and then spincoated 500 rpm in 1 minute + spin coated 3000 rpm in 20 seconds.

3.3.2 Beam size

The beam profile of the laser was Gaussian and the beam size is defined as the full width half maximum (FWHM) of the gaussian. In order to have a beam size covering the active area of the solar cell, the FWHM was measured at different distances relative to the laser source to find an appropriate position for the solar cell. A beam profiler was connected to the oscilloscope and placed after the pinhole (see figure 3.6, experimental set up). The timescale on the oscilloscope was selected such that the individual pixles on the detector of the beam profiler were clearly visible. The distance between the pixles was known to be 14 µm and by counting the number of detectors within a known timeinterval the timescale could be converted to a lengthscale. The FWHM of the beam profile was then measured in time and converted to beam diameter. The diameter of the solar cell was 2,26 mm and the chosen position had a beam size of 2.4 mm, see figure 3.5. The gray area is the part of the Gaussian which strikes the sample and this corresponds to 72% of the total area of the gaussian.

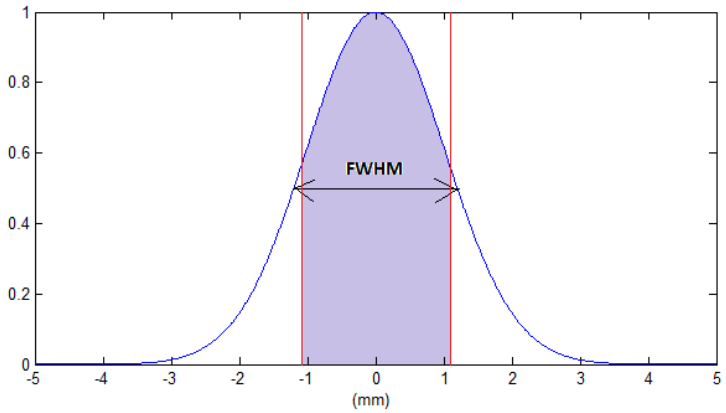

Figure 3.5: Beam profile illustrated with a Gaussian and the laser width is given by the FWHM. The red lines show the extension of the solar cell within the beam if placed in the center.

It should be noted that the distribution of radiation on the sample was inhomogeneous. On both edges of the sample the intensity was only 56% of the corresponding value at the center of the solar cell.

3.3.3 Power

The energy of a photon is given by $E = h \cdot 1/\lambda$ where λ is the wavelength and h is planck constant. With the laser wavelength λ=532 nm and photon energy, $E = 3.72 \cdot 10^{-19}\, J$ following relationship applied:

$$1\ sun = (8.25 \cdot 10^{16})\ \frac{\text{photons}}{\text{s} \cdot \text{cm}^2} \Leftrightarrow (8.25 \cdot 10^{16} \cdot 3.72 \cdot 10^{-19})\ \frac{\text{J}}{\text{s} \cdot \text{cm}^2} = 31\ \text{mW/cm}^2$$

The diameter of the solar cell was 2,26 mm and the active area, *A*, was therefore $A = \pi * 0{,}113^2\ cm^2 = 0{,}04\ cm^2$. For the fluence to be 1 *sun* on the solar cell the power on the active area had to be *1.24 mW*:

$$1\ sun = (31 \cdot 0{,}04)\ \text{mW} = 1{,}24\ \text{mW}$$

Because only 72% of the laser beam hits the sample the measured power in front of the solar cell (see figure 3.3) had to be 1,72 mW for the fluence to be 1 sun on the solar cell.

$$0{,}72 \cdot 1{,}72\ \mathrm{mW} = 1{,}24\ \mathrm{mW}$$

3.3.4 Experimental setup

The experimental setup is shown in figure 3.6. The samples were excited at 532nm. The laser source was a Nd-YAG laser, from ACE laser which generated laser pulses at 1064nm. The green 532 nm excitation source was produced by frequency doubling the 1064 nm beam using a second harmonic Beta barium borate (BBO) crystal.

The experimental work required a variation of the repetition rate of the laser. This was controlled by adjusting an external trigger which was done using a digital delay generator. The repetition rate was varied from 1000 Hz up to 25 kHz, which was the maximum repetition rate of the laser. The beam was focused onto the solar cell, which was placed at a distance where the size of the laser beam covers the active area of the sample. Before reaching the sample, the beam passed through a pulse energy filter, an IR-filter and finally a pinhole. The pulse energy filter was used to regulate the pulse energy of the beam impinging the solar cell. The IR-filter extracted any residual infrared light which was left from the second harmonic generation process. The pinhole was used to make the shape uniform and subtract scatter.

Upon laser excitation, the charges produced in the solar cell were extracted via the electrodes of the solar cell. These charges and therefore the response of the solar cell were analyzed by an oscilloscope which was connected to the electrodes. The oscilloscope displayed the voltage as a function of time and the voltage- and timescales were adjusted such that the entire voltage response was incorporated (see figure 3.8). The collected data were averaged over 2000-3000 pulses by the oscilloscope before it was stored as a text file. The oscilloscope had an inner resistance equal to 50 ohm.

A power meter was used to measure the intensity of the beam which impinged the sample. The intensity registered was a mean value of measured intensity before and after the voltage response of the solar cell was collected in the oscilloscope. The measurements on very low energies per pulse were measured in dark, due to the weak response of the solar cell.

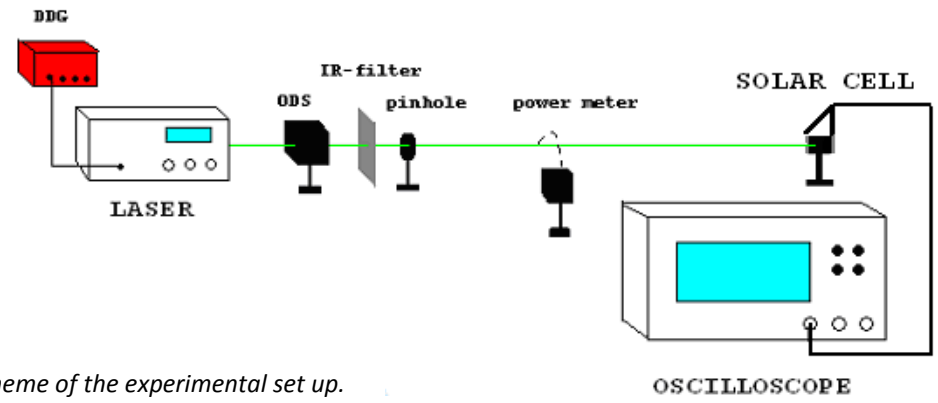

Figure 3.6: Scheme of the experimental set up.

3.3.5 Signal to noise

Even though no light impignes the solar cell, the oscilloscope connected to the solar cell will have a certain background noise due to thermally energy fluctuations ~k_BT. It follows that a voltage corresponding to a smaller energy than these energy fluctuations will not be detectable. The signal to noise increases with number of measurements, and cons*eqe*ntly different repetition rates of the laser when measuring over a specific time interval will give different signal to noise. Best signal to noice is accuired for high repetition rates. In the experiment less pulses were averaged when the solar cell response was measured for lower repetition rates, since more time was required. If the number of measurements equals *n*, the signal to noise improves with a factor proportional to $\sqrt{n}$. This should be beared in mined when analyzing the results.

Since signal to noise is a measure that compares the level of the desired signal to the level of background noise, its natural that measurements with larger pulse energies will give a better signal to noise.

Part 2

3.4 Software

A large part of the analyse program was made before the measurements. Similar measurements had been done before and therefore old data was used for the programming. The old data contained a high degree of electrical noise which garantied that the program would work with measurements of the same extent of white noise or less.

3.4.1 Head program

In the head program the *EQE* was calculated and the solar cell current decay was fitted using the collected data from the experiment. The scheme for the head program is shown in figure 3.7. In the program the voltage response from the sample (1) was processed with a function *DataProcessing* to arrive with data which could be easily refined in following computations. The number of electrons extracted from the sample was calculated with a function *IntegrationOfData* and the solar cell discharge was fitted with assistance of the function *ExponentialFitting*. The number of photons impinging on the sample was calculated with the function *PhotonPerpulse* based on the frequency (2) and the measured power (3) of the laser applied in the experiment.

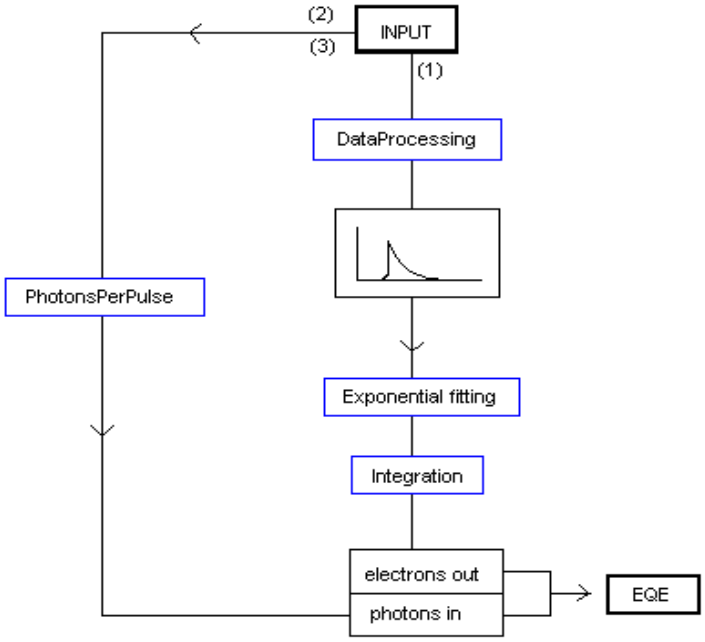

Figure 3.7: Scheme of the head program. The blue boxes illustrate the different functions used in the program. The inputs are the voltage- and time-vector (1) measured with the oscilloscope, the frequency (2) of the laser and the measured power (3) of the light in front of the solar cell.

3.4.2 Data processing

The inputs to the function *DataProcessing* were the voltage vector $V$and the time vector T. These variables were sampled with the oscilloscope and therefore the settings of the oscilloscope and the connection between the oscilloscope and electrodes influenced their values. A typical set of data is plotted in figure 3.8 with voltage on the vertical axis and time on the horizontal axis.

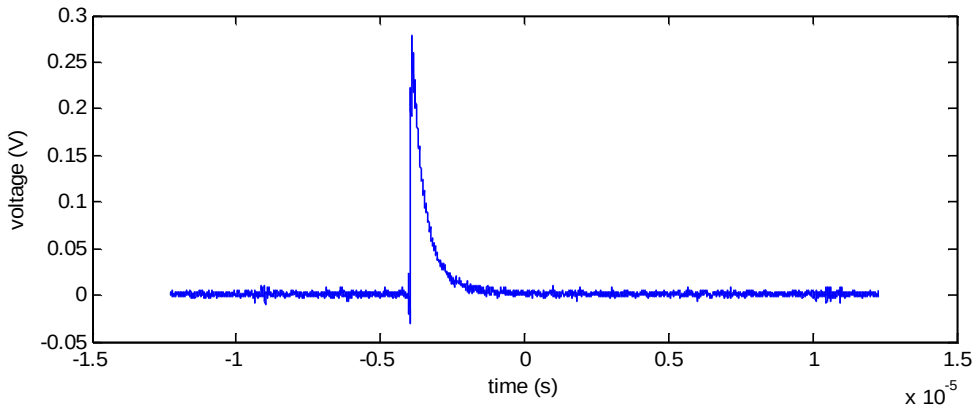

Figure 3.8: Typical plot of a data set collected with the oscilloscope. The peak shows the voltage response from the solar cell when hit by a flash of light.

The aim with the function data processing was to arrive with data of similar properties which could be easily processed in following computations.

Different Initial conditions were being considered:

- An average background voltage different from zero.
- A negative voltage response due to opposite connections of the electrodes to the solar cell.

The three steps of the data processing function:

1. Put the average background voltage to zero.
2. Change the voltage data to current data.
3. Convert a negative current response into a positive.

The *first* step was performed by use of statistics. The aim was to move the data in vertical line to end up with an average background voltage equal to zero.

By studying where the voltage drastically raised (see for example figure 3.4 at time -0.4 µs) an average value on the background voltage could be computed based on the elements ahead. For this purpose the mean value, μ, and the estimator of the standard deviation, s, were used.

$$\mu = \frac{1}{N}\sum_{i=1}^{n} x_i$$

$$s = \sqrt{\sum_{i=1}^{n} \frac{1}{N}(x_i - \mu)^2}$$

In this calculation x_i is the i:th element of the voltage vector, *V*.

μ and s were calculated based on the first 100 elements in *V* which were assumed to be part of the background noise. These variables were then applied in a while-loop where the ratio, *r*, between the average deviation, *d*, and the estimator of standard deviation, *s*, was conditioned. The average deviation from the mean value was calculated with twenty subsequent elements:

$$d = \sum_{i=k}^{k+19} \frac{1}{20} abs(x_i - \mu)$$

An experimental approach showed that if the ratio, *d/s*, was larger than three, some elements included in the calculation were taking part of the voltage rise. The condition in the while-loop was based on this experimental information.

In figure 3.9 a scheme over the while-loop is shown. *k* is an index which keep track on the element in the voltage vector and *D* is a tool for calculating the average deviation *d*.

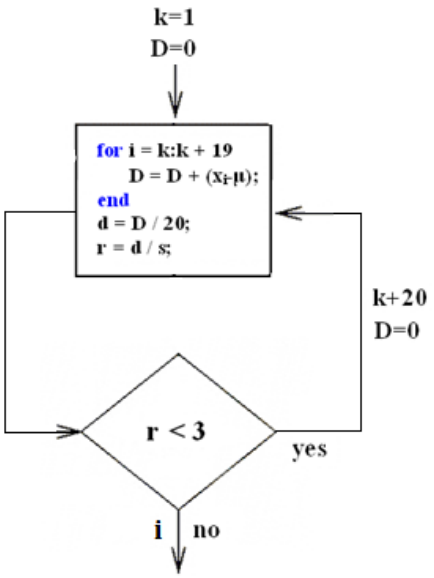

Figure 3.9: Scheme of while loop. Input values are k=1 and D=0. To calculate the average deviation d, a variable D is introduced. If the ratio r=d/s is smaller than three the loop walks on to the next twenty elements in the voltage vector. If the ratio is larger than three the loop stops and returns an index i representing an element in the voltage vector which is part of the voltage response from the solar cell.

The loop returned an element *i* which was part of the voltage response of the solar cell. This element was then subtracted with 20 and multiplied with 0.8 to arrive with an element, *j*, close to the rise, but not part of it. The average background voltage, $V_{background}$, was then calculated based on the elements ahead of element *j*. The corrected voltage vector, V_0, was found by subtracting the original voltage vector *V* with the calculated background voltage.

$$V_{background} = \frac{\sum_{i=1}^{j} x_i}{j}$$

$$V_0 = V - V_{background}$$

In the *second* step V_0 was converted to a current vector, I_0. The oscilloscope had an inner resistance of 50 ohm and the computations made followed directly from Ohms law: $I = U/R$. Each element in the voltage vector was divided by 50 to arrive to the current vector.

In the *third step* negative current responses was converted into positive. Since the data sometimes were quite noisy smoothing was necessary, see red curve in figure 3.10. If the mean value of the smooth current vector was negative the sign of all elements was shifted.

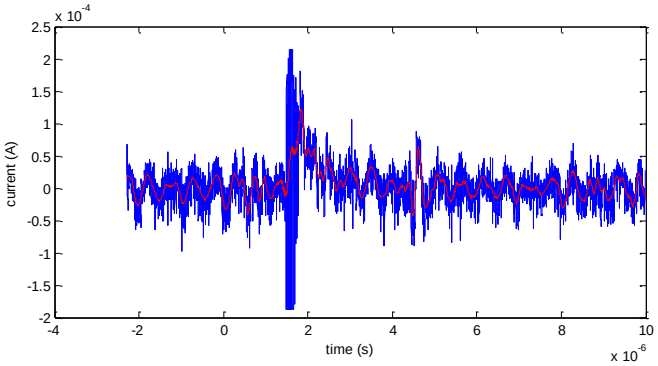

Figure 3.10: Blue: Raw data. Red: Smoothed data. The noise on the rise is due to electrical noise measurement.

The smoothing was made with a Savitzky-Golay filter with frame size 201 and polynomial of second degree. This type of smoothing is used throughout the program.

3.4.3 Exponential fitting

The exponential fitting was performed in the head program with the assistance of the function *ExponentialFitting*.

The structure of the exponential fitting function *f(t)* is shown below:

$$f(t) = C_0 + C_1 \cdot e^{-k_1 t} + C_2 \cdot e^{-k_2 t} + \ \ldots$$

Where k_1, k_2, … are the rate constants, C_0, C_1, C_2, … are the coefficients and t is the time. The reason why *f(t)* is chosen to include a constant is to minimize errors due to a background level separate from zero.

Sub vectors of the current- and time vector were created which started where the original smoothed current vector had its maximum value, see figure 3.11. The smoothed current vector is illustrated as a red line in figure 3.11 (A) together with the raw data (blue). The sub vectors *t* (time) and *Z* (current) are shown together in figure 3.11 (B).

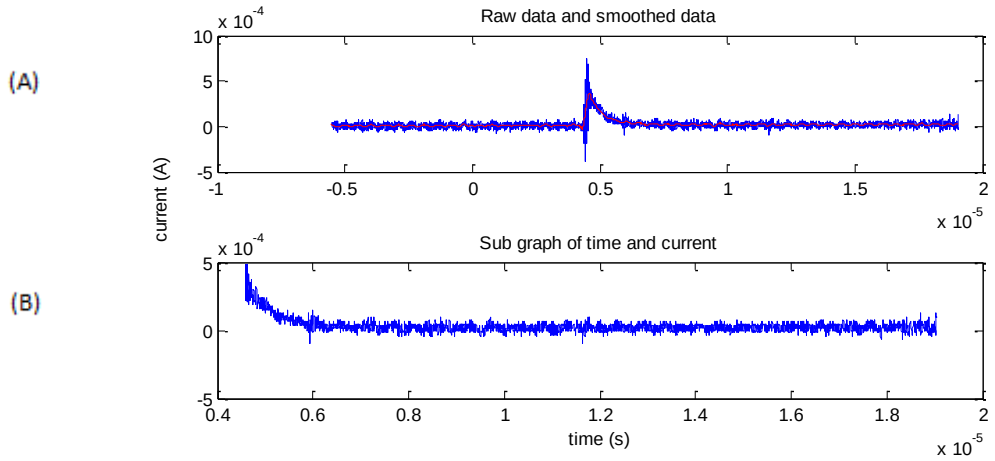

Figure 3.11: (A) Blue: raw current data. Red: smoothed current data. (B) sub vector, Z, of the current vector I_0 and sub vector t, of the time vector T. Both sub vectors start where the original smooth current data has its maximum value.

The input to the function *ExponentialFitting* was *Z*, *t* and a vector of rate constants. The number of rate constants in the input was chosen depending on how many exponentials were preferred for the exponential fitting function. Based on the inputs the coefficients were calculated by solving the normal equation (see below) and a measure of the deviation of the exponential fit from the observed data was returned.

The rate constants which minimized the output from function *ExponentialFitting* were found by using a matlab function called *fminsearch*. The command *x = fminsearch (ExponentialFitting ,x0)* started at the point *x0* and returned a value *x* that was a local minimizer of the function *ExponentialFitting*. The hypothetical values of the rate constants was put in as *x0* and the values returned from fminsearch were consequently the rate constants which were local minimizers of the deviation of the experimental fit from the observed data.

To arrive with the exponential fit function it remained to calculate the coefficients. This was done by using the known rate constants given from the fminsearch command. The same method that is shown here was also used in the function *ExponentialFitting* to calculate the coefficients in the exponential fitting function.

To simplify the matter only two rate constants are considered. The same approach can be used for a larger amount of rate constants. Now, *f(t)* can be written as following:

$$f(t) = Ax$$

Where $A = \begin{bmatrix} 1 & e^{-k_1 t_1} & e^{-k_2 t_1} \\ 1 & e^{-k_1 t_2} & e^{-k_2 t_2} \\ 1 & e^{-k_1 t_3} & e^{-k_2 t_3} \\ \vdots & \vdots & \vdots \end{bmatrix}$ and $x = \begin{bmatrix} C_0 \\ C_1 \\ C_2 \end{bmatrix}$

The closest fit is obtained when *Ax* is as close to the observed data, *Z*, as possible. Therefore *x* is solved for:

$$Ax = Z$$

This equation system has more equations than unknown and cannot be solved in general. Instead the normal equation is solved:

$$A^T Ax = A^T Z$$

Number of exponentials for the fitting function

The number of exponentials used to fit the function was decided by a visual comparison of the fit and the raw data. Two exponential functions were decided to be enough for fitting the data and therefore two exponentials were used in the alternative integration method found in next section. After the measurements were done, a closer analysis lead to the conclusions that three exponential functions gave the closest approximation to the current decay in the solar cell device (see result part).

3.4.4 Integration of data

The number of electrons extracted from the solar cell was calculated with the function *Integration*. The input to the function was the current vector I_0 (see section 3.2.1 Data Processing) and the original time vector *T*. To arrive with the total charge, *Q*, corresponding to the response of the solar cell after excitation, a regular integration was made by dividing the current curve into rectangles with height y_i and thickness Δt_i.

$$I(t) = \begin{cases} y_1 & when\ t_1 \leq t \leq t_2 \\ y_2 & when\ t_2 < t \leq t_3 \\ & \vdots \\ y_{n-1} & when\ t_{n-1} < t \leq t_n \end{cases}$$

$$y_i = (x_{i+1} + x_i)/2$$

$$\Delta t_i = (t_{i+1} - t_i)$$

where x_i is the value of I_0 in element *i* and t_i is the value of *T* in element *i*. The sum of all rectangles is the total charge, Q, which corresponds to the total amount of electrons extracted from the solar cell.

$$Q = y_1 \cdot \Delta t_1 + y_2 \cdot \Delta t_2 + \cdots + y_{n-1} \cdot \Delta t_{n-1}$$

Number of electrons

Number of electrons in the pulse was found by dividing Q with the elementary charge.

$$\#electrons = Q/q$$

$$q = 1.602 \cdot 10^{-19}\ C$$

Alternative integration method

An alternative way of integrating the data was evaluated. This was based on the exponential fit *f(t)* of I_0, found with the function *exponential fitting*. This method wouldn't require that each element in the current vector was treated and therefore this method would enable fast computations even with lots of data. In this method *I(t)* is the exponential function *f(t)* without the constant C_0. *I(t)* was

extrapolated backwards to start at time t_0 where the smooth current curve had a value corresponding to 60% of its max value. t_n is the final element in the time vector t. The total charge is approximated to be the integral of this function.

$$I(t) = C_1 e^{-k_1 t} + C_2 e^{-k_2 t}$$

$$Q = \int_{t_0}^{t_n} I(t) \cdot dt$$

Since *I(t)* was known, *Q* could be computed with an integration function in MATLAB.

For this method to be correct the integrated exponential function should have a value in close approximate to the integration made directly from the raw data. It was found that for some data this was not true. With high background level the exponential fit could decline steeply at the top of the current curve as seen in figure 3.12. The extrapolation back in time was consequently raised to high current values and it followed that the integral of the extrapolated exponential function was much larger than the corresponding integrated raw data. This observation resulted in the choice of integration of raw data.

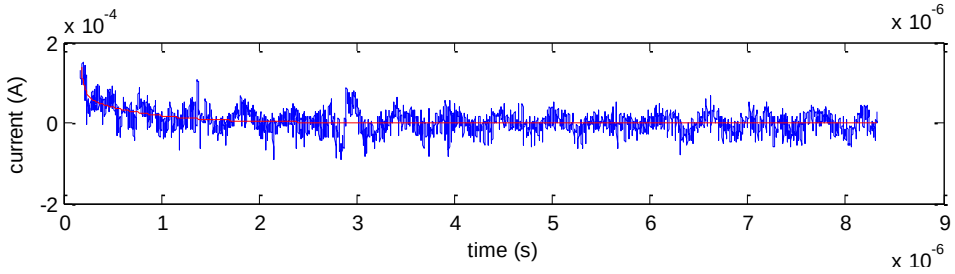

Figure 3.12: Blue: raw data. Red: exponential fit. Extrapolation back in time would result in high current values.

3.4.5 Photons per pulse

The number of photons per pulse was calculated based on the frequency, wavelength and the power of the laser applied in the experiment.

The energy per photon was calculated with the Planck-Einstein equation and according to earlier result (see section 3.3.3 Power) the photon energy was $3.72 \cdot 10^{-19}$ J.

To calculate the energy per pulse, E_{pulse}, the averaged power, P, on the solar cell was divided by the applied frequency, f, of the laser. The number of photons per pulse were then found by dividing the energy per pulse with the photon energy.

$$\frac{P[\frac{\mathrm{J}}{\mathrm{S}}]}{f[\mathrm{s}^{-1}]} = E_{pulse}[\mathrm{J}]$$

$$\#photons\ per\ pulse = E_{pulse}[\mathrm{J}]/hv$$

Since the laser beam had a larger cross-section area than the active material of the solar cell the measured power had to be multiplied with a factor 0.72 to arrive with the power, *P*, on the solar cell (see section 3.2.2 Beam Size).

3.4.6 Analysis of the exponential fitting of the measured data

The analysis of the exponential fitting of the measured data was made by studying the residual, *e*, which is the difference between the observed current, Z, and the fitted exponential function, $f(t)$.

$$e_i = z_i - f(t_i)$$

where *i* is the index for the position in the vectors.

The residual was studied for different repetition rates and pulse energies for both the APFO3:PCBM sample and the TQ1:PCBM60 sample.

4 Results

4.1 APFO3:PCBM

The result from the measurement of the *EQE* is shown as a function of energy per pulse for the APFO3:PCBM combination in figure 4.1. Different repetition rates are illustrated with different marks and colors. It's observed that the *EQE* decreases over the measured range of energy apart from the *EQE* at very low energies. Regardless of repetition rate the data points of the *EQE* forms a single curve. Only the data which appertain to measurements of repetition rates 1000 Hz and 5000 Hz seem to deviate from the rest at lower pulse energy. The maximum value of the *EQE* is 6 % and the decrease of the *EQE* starts when the energy per pulse is approximately 10^{11} *hv*/cm^2.

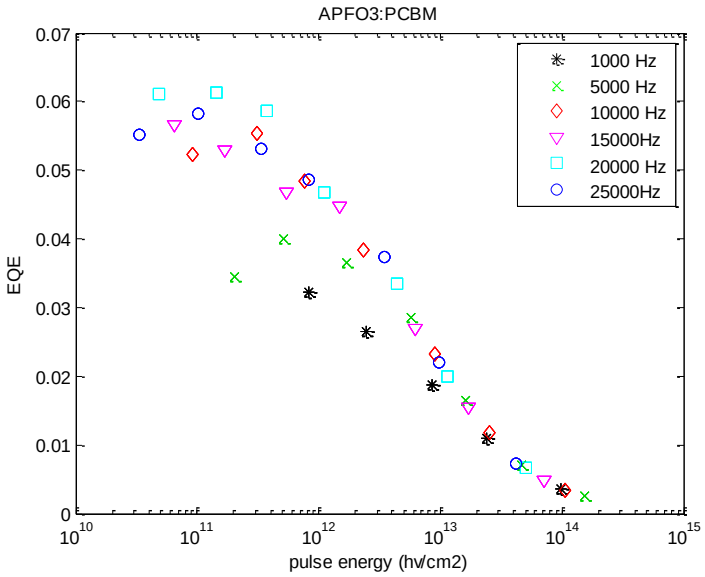

Figure 4.1: EQE as a function of energy per pulsed for APFO3:PCBM.

4.2 TQ1:PCBM60

The results of the *EQE* as a function of energy per pulse are shown for the TQ1:PCBM60 combination in figure 4.2. Also in this type of solar cell the *EQE* from different frequency measurements approach a single curve at higher energies per pulse. For lower energies the data of the *EQE* are more disseminated as also could be seen for the APFO3: PCBM combination. Although the *EQE* of the higher frequencies follow each other quite well at low energies, the data originating from repetitions rates 1000 Hz and 5000 Hz deviate from the rest. The maximum value of the *EQE* is approximately 5.5 %.

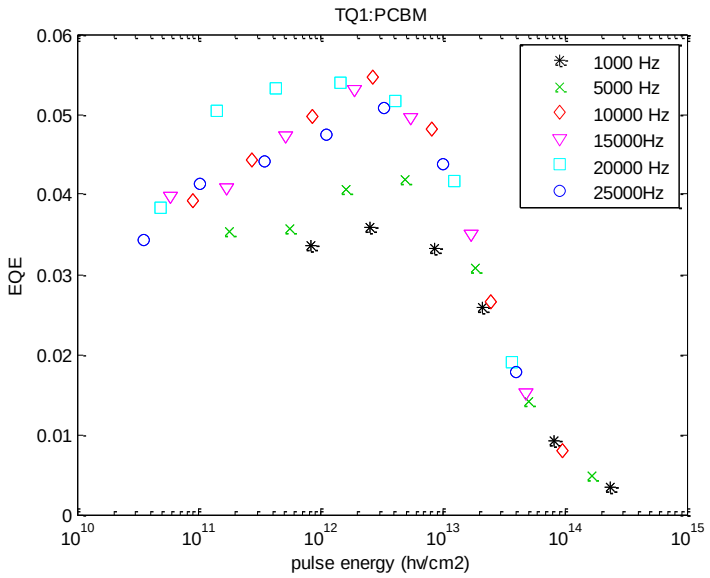

Figure 4.2: EQE as a function of pulse energy for TQ1:PCBM60.

It appears that the *EQE* for all repetition rates increase when the energy increases in the beginning of the interval, although the signal to noise in this part of the measurements is far from perfect. Somewhere between 10^{12} *hv*/cm^2 and 10^{13} *hv*/cm^2 the trend changes and the *EQE* starts to decrease.

Thus, both diagrams showed that observations originating from different repetition rates approached a single curve when the pulse energy increased. For lower pulse energy the data were more dispersed due to lower signal to noise, especially for the data appertaining to the lowest repetition rates. Disregarding the data measured with repetition rate 1000 Hz and 5000 Hz the *EQE* from different repetition rate follow each other quite well also in the range of low pulse energies. This indicates that repetition rate has a minor importance when it comes to conversion of photons into electrons. Consequently, this support that the solar cell doesn't need to form an electric equilibrium of photo generated charges to optimize the performance of the solar cell; space charge doesn't influence the cell performance in this range of repetition rates.

For both types of solar cells the *EQE* diminished with higher pulse energy after a certain critical value, which was 10^{11} *hv*/cm^2 for APFO3 and somewhere between 10^{12} *hv*/cm^2 and 10^{13} *hv*/cm^2 for TQ1. Thus, pulse energy is substantial for the solar cell functioning. For TQ1 there seemed to be an increase of the *EQE* in the beginning of the pulse energy interval, but as mentioned before the signal to noise is low here and consequently this doesn't have to originate in the physics of the device. At pulse energies shortly above 10^{14} *hv*/cm^2 the ratio between extracted electrons and photons incident on the solar cell approached zero for both samples and thus there exists a higher limit for solar cell operation conditions regarding pulse energy. In the range for which the pulse energy was varied no lower limit for solar cell operation conditions was observed. The extension of the *EQE* to lower pulse energies is not obvious, but the impression is that the *EQE* doesn't increase further.

Keep in mind that the pulse energies displayed in the figures are averaged values of the concentration of photons incident on the sample. Since the laser beam had a Gaussian shape the concentration of photons in the center of the beam was larger than the average concentration.

4.3 Exponential fitting of measured data

In order to investigate the condition for nongeminate recombination to largely contribute, the current response from the solar cell was fitted with an exponential function. As mentioned in the theory part the solar cell discharge most probably is exponential if the contribution from nongeminate recombination could be neglected.

The closest fit to the measured data for both samples was found with an exponential function, *Y*, consisting of one constant and three exponentials. The constant C_0 was close to zero for all fitting functions since the background level of the voltage was set to zero in the function *DataProcessing.*

$$Y = C_0 + C_1 e^{-k_1 t} + C_2 e^{-k_2 t} + C_3 e^{-k_3 t}$$

The fitting results for different pulse energies at a repetition rate of 10 000 Hz is shown in figure 4.1 and 4.2 for APFO3 and TQ1 respectively.

Table 4.1: Constants from the fitting results of APFO3 at a repetition rate of 10 000 Hz.

Energy (*hv*/cm^2)	**C_0**	**C_1**	**k_1**	**C_2**	**k_2**	**C_3**	**k_3**
9.28e+10	-5.77e-7	8.38e-5	5.21e+6	4.53e-6	6.63e+5	1.36e-6	3.14e+4
3.13e+11	-1.81e-6	2.91e-4	5.19e+6	1.72e-5	6.47e+5	4.39e-6	3.03e+4
7.69e+11	1.10e-6	1.37e-3	5.09e+6	1.32e-4	8.56e+5	1.61e-5	1.12e+5
2.31e+12	2.39e-7	6.15e-4	5.27e+6	4.37e-5	7.59e+5	6.79e-6	8.84e+4
9.14e+12	6.62e-6	2.33e-3	4.76e+6	6.51e-4	1.35e+6	7.49e-5	2.68e+5
2.55e+13	9.27e-6	2.06e-3	4.25e+6	1.37e-3	1.65e+6	1.52e-4	3.57e+5
1.06e+14	-3.62e-6	3.31e-3	2.44e+6	4.33e-4	6.93e+5	3.97e-5	7.09e+4

Table 4.1: Constants from the fitting results of TQ1 at a repetition rate of 10 000 Hz.

Energy (*hv*/cm^2)	**C_0**	**C_1**	**k_1**	**C_2**	**k_2**	**C_3**	**k_3**
9.23e+10	-2.40e-7	1.34e-5	3.39e+6	3.29e-6	6.26e+5	1.67e-6	7.35e+4
2.83e+11	7.54e-7	5.51e-5	4.46e+6	1.36e-5	9.07e+5	6.14e-6	1.56e+5
7.55e+11	1.85e-6	1.61e-4	3.69e+6	3.82e-5	7.04e+5	2.12e-5	1.37e+5
2.02e+12	3.92e-6	4.73e-4	2.62e+6	1.22e-4	5.55e+5	7.91e-5	1.53e+5
8.41e+12	1.95e-7	1.32e-3	2.12e+6	4.93e-4	5.27e+5	1.47e-4	1.33e+5
2.28e+13	6.98e-6	2.5e-3	1.73e+6	5.39e-4	5.05e+5	3.19e-4	1.86e+5
8.17e+13	-3.00e-6	3.08e-3	1.56e+6	6.76e-4	3.56e+5	1.42e-4	1.06e+5

The residuals (see section 3.4.6 Analysis of the exponential fittings of the measured data) calculated with the exponential function, *Y*, was distributed randomly around zero for measurements done with low excitation energies. This implies that the exponential fit is a good approximation for the solar cell discharge at low excitation energies. The exponential fit and the residual is shown in fig. 4.3 for the TQ1 sample, when the frequency was 10 000 Hz and pulse energy was $2.02 \cdot 10^{12}$ *hv* /cm^2.

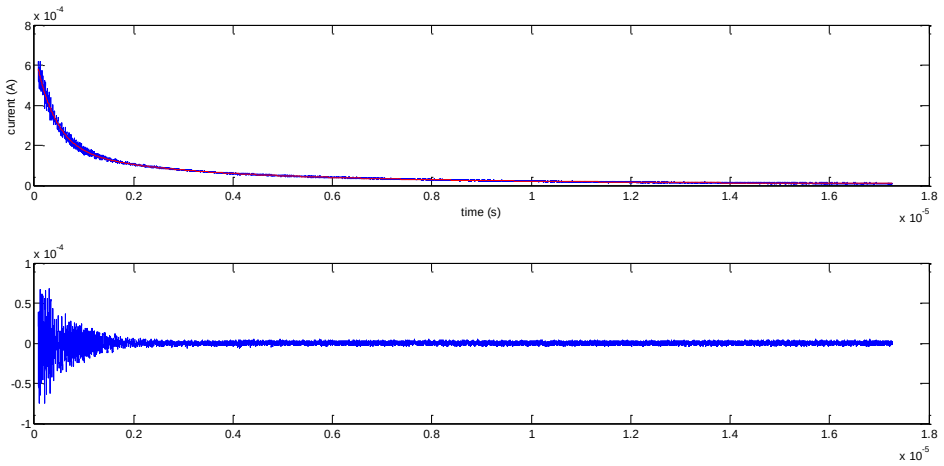

Figure 4.3: Residual of the TQ1:PCBM combination at a frequency of 10 000 Hz and pulse energy equal to $2.02 \cdot 10^{12}$ hv/cm^2. The residual data is distributed almost symmetrical around zero.

For the slightly larger pulse energy, $8.41 \cdot 10^{12}$ *hv*/cm^2, still same frequency, the residual show some structure which implies that the solar cell discharge can no longer be simulated with an exponential function, see figure 4.4.

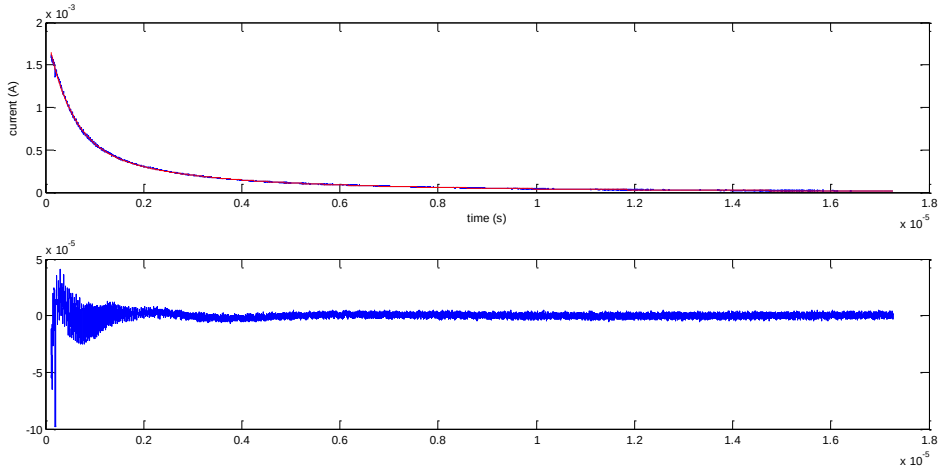

Figure 4.4: Residual of the TQ1:PCBM combination at a frequency of 10 000 Hz and pulse energy equal to $8.41 \cdot 10^{12}$ hv/cm^2. The residual data is no longer distributed symmetrical around zero.

For the APFO3 sample the deviation from a symmetric residual started at the energy slightly above 10^{11} *hv*/cm^2 per pulse.

Hence, for both solar cells the current decay was approximately exponential for light impinging the solar cells had low pulse energies. At higher pulse energies the residuals were not symmetric distributed around zero, probably originating in a stronger contribution from the nongeminate recombination. An important observation is that the pulse energy for which the *EQE* starts to decrease (see fig. 4.1 and 4.2), at 10^{11} *hv*/pulse for APFO3 and between 10^{12} and 10^{13} *hv*/pulse for TQ1, energies also associated with the limits for which the current decay can be simulated with an exponential decay. Thus, the *EQE* starting to decrease also means nongeminate recombination getting stronger.

5 Discussion and conclusions

5.1 Low *EQE*

The maximum *EQE* obtained for APFO3:PCBM was 6 % and for TQ1:PCBM60 5.5 %. Both values are low, for the *EQE* at short circuit condition.

The excitation wavelength was 532 nm and it is within the absorption range of both samples. Yet the absorption can be a limiting factor for the *EQE* as the thickness of the active material in the cells was on the order of 100 nm. Errors in the determination of the power input to the solar cell may also affect the value of the *EQE*. Since the laser beam had a Gaussian shape, an error in the measured beam size would contribute to an even larger error in the cross-section of the Gaussian. Consequently, the error in the calculated ratio between the solar cell cross area and the Gaussian cross area will influence the *EQE*. This error is however not enough to alone explain the much lower *EQE* values than expected.

Another possibility is that the method and accuracy of the instruments were insufficient for this experiment. If the current through the solar cell extended over a long time period, some part of the response may have been missed in the analysis. The accuracy of the oscilloscope may also have been too low to detect these small currents even though incorporated in the analysis and consequently a significant part of the voltage response may be undetected. A poor time response from the oscilloscope would also risk that information of processes on smaller timescales would not be observed.

Finally it may be emphasized that cell functioning using pulsed light may be different from that of steady state. Pulsed light means a higher instantaneous concentration of light, and thus the performance may differ. Degradation of the active material in the solar cell is probably of minor importance.

The small *EQE* value which occurred for both type of solar cells may thus have several explanations. Substantial effects on the results may arise with insufficient accuracy of the oscilloscope. If the solar cell functioning is different from steady state conditions, this may also largely influence the *EQE*. However, it's assumed that the *EQE* is lowered by the same factor for all different excitation condition.

5.2 *EQE* and pulse energy

The results from section 4.1 and 4.2 revealed that the pulse energy was substantial for the *EQE*. For high energies the *EQE* drastically declined and this is accredited to non geminate recombination. Since geminate recombination is a first order process proportional to the electron (hole) concentration, the ratio will remain the same between regeneration of bound pairs and geminate recombination. However, non geminate recombination is a second order process, proportional to the squared electron (hole) concentration and it follows the *EQE* will decrease when non geminate recombination is getting strong. The result from section 4.3 further strengthened the assumption that non geminate recombination was the limiting factor for solar cell functioning at high pulse energies.

The pulse energies for which the non geminate recombination became visible were different for the two types of solar cells that were investigated and this is assumed to be related to different morphology of the active material. For sufficiently high pulse energy it was shown that the conversion efficiency of both samples approached zero. This is because the incident photons contributed to such a high concentration of holes and electrons that almost all charge carriers recombined before reaching their respective electrode. This means that there is a higher limit for solar cell operation regarding pulse energy. No limitation of solar cell operation due to too small pulse energy could be observed in the measured range of pulse energies and the dispersed data in the range of low pulse energies obstruct assumptions about the extension of the *EQE* to lower pulse energies. Therefore it's not possible to say whether a solar cell will work with the same efficiency on a single photon as for normal sun lightning.

5.3 *EQE* and repetition rate

The repetition rate turned out not to be substantial for the solar cell operation in this experiment. In both figure 4.1 and 4.2 the values of the *EQE* followed a single curve at high energies per pulse independent of which repetition rate the measurements was performed with. At low energies the low frequencies deviated from the rest, but this may be correlated with the larger error in this measurement region. Nevertheless, it's not excluded that there may be some physical explanation for the lower *EQE* at these frequencies.

The result was interpreted as no quasi-equilibrium of photo generated charges needed to be established in the solar cell in order to optimize the conversion efficiency. However, the measurements were restricted to a specific interval of repetition rates and thus it can't yet be excluded that there are no photo generated charge carrier distribution which may favor the conversion process.

5.4 Improvements

To minimize the difference in photon concentration incident on the sample, due to the Gaussian laser beam, the solar cell could have been placed further away from the laser source. With a broader beam the solar cell could be fitted in the middle of the Gaussian where the energy was more or less constant. This would give a more accurate result and minimize undesirable drift due to concentration gradients.

To know what factor limited the *EQE* it would be best to measure the *IQE*. The *EQE* would show if the absorption was the main limiting factor and would eliminate one uncertainty.

5.5 Outlook

Both repetition rate and pulse energy was in this experiment restricted to a specific interval. In order to fully exclude the possibility that the solar cell may work more efficiently with some incident distribution of photo generated charge carriers in the solar cell, the repetition rate should be varied from those in this study up to repetition rates approaching that of continuous light.

Regarding pulse energy we found that there most probably is a higher limit for solar cell operation condition. In order to evaluate if the solar cell works with the same efficiency for a single photon

compared to normal sun conditions, it may be interesting to extend the measured pulse energies to even lower values. However, more accurate instruments are needed to see any significant response from the solar cell at these low pulse energies.

Acknowledgments

I would like to gratefully thank my supervisors Arkady Yartsev and Dimali Vithanage for advice, help and patience through my work. Thanks to Yingyot Infahsaeng who kindly helped me with all sorts of problem and Torbjörn Pascher for showing me the instruments in the lab. Finally I would like to say thank you to my partner Marcus and my friends for supporting me during my project.

References

[1] Serkan Toto, Mitsubishi Chemical To Commercialize Printable Solar Cells Next Year, April 6th, 2011. http://techcrunch.com/2011/04/06/mitsubishi-chemical-to-commercialize-printable-solar-cells-next-year/ (brought 2012-04-16)

[2] Harald Hoppe, N. Serdar Sariciftci. *Polymer Solar Cells*. Advanced Polymer Science. 2008, 214, 1-86

[3] Paul W. M. Blom, Valentin D. Mihailetchi, L. Jan Anton Koster, and Denis E. Markov. *Device physics of Polymer: Fullerene Bulk Heterojunction Solar Cell.* Adv. Mater. 2007, 19, 1551-1566.

[4] S. Günes, H. Neugebauer, N. S. Sariciftci Chem. *Conjugated Polymer-Based Organic Solar Cells*. Chemical Reviews, 2007, Vol. 107, No 4, 1324-1338.

[5] Adam J. Moulé. *Power from Plastic*. Chemical Engineering and Materials Science Department. University of California Davis, 1 Shields Ave., Davis, CA 95616, United States. Accepted 16 June 2010. Received 5 Feruary 2010.

[6] Valentin D. Mihailetchi, Hangxing Xie, Bert de Boer, L. Jan Anton Koster, Paul W.M. Blom. *Charge transport and photocurrent generation in poly(3-hexylthiophene):Methanofullerene bulk-heterojunction solar cells*. Adv. Funct. Mater. 2006, Vol 16, 699-708.

[7] G. Yu, J. Gao, J. C. Hummelen, F. Wudl and A. J. Heeger. *Polymer Photovoltaic Cells: Enhanced Efficiencies via a Network of Internal Donor-Acceptor Heterojunctions.* Science 1995, vol. 270, 1789-1791.

[8] Almantas Pivrikas, Helmut Neugeauer, Niyazi Serdar Sariciftci. *Charge Carrier Lifetime and Recombination in Bulk Heterojunction Solar Cell*. IEEE journal of selected topics in quantum electronics 2010, Vol 16, No 6.

[9] Dipl.Ing. Klaus Petritch. *Organic Solar Cell Architectures*. PhD thesis. University of Cambridge, UK and Technische universität Graz, Austria, 2000.

[10] L.J.A. Koster, E.C.P. Smits, V.D. Mihailetchi, P.W.M. Blom. *Device model for the operation of polymer/fullerene bulk heterojunction solar cells*. Physical review 2005, B 72, 085205.

[11] Blog based on [Langevin 1903 (Ann. Chim. Phys. 28, 433)]. Updated 3.12.2008 http://blog.disorderedmatter.eu/2008/04/04/recombination-in-low-mobility-semiconductors-langevin-theory/ (Brought 2012-01-15).

[12] Swati De, Torbjörn Pascher, Manisankar Maiti, Kim G. Jespersen, Tero Kesti, Fengling Zhang, Olle Inganäs, Arkady Yartsev, Ville Sundström. *Geminate Charge Recombination in Alternating Polyfluorene Copolymer/Fullerene Blends*. J. AM. CHEM. SOC. Vol. 129, No. 27, 2007.

[13] American Society for Testing and Materials (ASTM), ASTM G159-98. http://www.astm.org/Standards/G159.htm (Brought 2011-08-15).